Journal of Molecular Liquids 293 (2019) 111432

Contents lists available at ScienceDirect

Journal of Molecular Liquids

journal homepage: www.elsevier.com/locate/molliq

Mixed convection boundary layer flow and heat transfer over a vertical plate embedded in a porous medium filled with a suspension of nano-encapsulated phase change materials

M. Ghalambaz [a,b], T. Groşan [c], I. Pop [c,*]

[a] Department for Management of Science and Technology Development, Ton Duc Thang University, Ho Chi Minh City, Vietnam
[b] Faculty of Applied Sciences, Ton Duc Thang University, Ho Chi Minh City, Vietnam
[c] Faculty of Mathematics and Computer Science, Babeş-Bolyai University, 400084 Cluj-Napoca, Romania

ARTICLE INFO

Article history:
Received 16 May 2019
Received in revised form 4 July 2019
Accepted 23 July 2019
Available online 01 August 2019

Keywords:
Porous media
Nano-encapsulated phase change materials (NEPCMs)
Boundary layer
Dual solution
Heat-transfer enhancement

ABSTRACT

The flow and thermal behavior of nano-encapsulated phase change materials (NEPCMs) dispersed in a liquid is investigated over a vertical flat plate. The NEPCM particles are consist of an encapsulation shell and a core made of phase change materials (PCMs). When the temperature of the liquid around the NEPCM particle is higher than the fusion temperature of the PCM core, the PCM core absorbs a notable amount of heat (the latent heat of the phase change) from the host fluid and melts. The vertical plate is embedded in a porous medium, and the porous medium is saturated with the suspension of NEPCM. There is a uniform flow over the plate, which can aid or oppose the natural convection flow over the plate. The partial differential governing equations for the flow and heat transfer of NEPCM suspension are introduced and transformed into a high order boundary value ordinary differential equation. The finite difference method with a colocation technique as the grid adaptation and automatic error control is utilized to integrate the governing equations. Validations are performed by comparing the results with the literature. It is found that there are two solution branches in the case of high opposing flows. The results indicate that the presence of NEPCM particles enhances the heat transfer over the plate. The decrease in the fusion temperature of NEPCM cores enhances the heat transfer.

1. Introduction

Many engineering applications are concerned to combine convective heat transfer in fluid-saturated porous media. The interest in this topic has been encouraged, to a great extent, due to the considerable applications of thermally driven flows in porous media in engineering areas such as civil, chemical, and mechanical engineering. Applications include electrochemistry, geophysical systems, food processing and storage, fibrous insulation, nuclear reactors, solar power collectors, geothermal applications, thermal insulation of buildings, the design of pebble bed nuclear reactors, metallurgy, underground disposal of nuclear or non-nuclear waste. The mixed convection flow past a flat surface placed in a saturated porous medium or through a channel filled with a porous medium is one of the fundamental problems concerning heat transfer in porous media. Comprehensive reviews of heat transfer mechanisms in geothermal systems have been first presented by Cheng [1,2] and Bejan [3]. Since then a large number of applied applications, both environmental and industrial, have triggered a swift extension of the research, and an extensive number of papers have been published related to the flow past surfaces of various flow configuration models. Pop and Ingham [4], Ingham and Pop [5–7], Nield and Bejan [8], Bejan et al. [9], Vafai [10,11], Vadász [12] and Bear [13] identified many applications that highlight the directions where further experimental and theoretical investigations and developments are essential.

There are several published papers related to the analysis of free and mixed convection flow past a vertical flat plate embedded in a fluid-saturated porous medium. We mention here only the following: Merkin [14,15], Cimpean et al. [16], Merkin and Pop [17], Merkin et al. [18], Lok et al. [19].

In the past several years, nanofluids have received much attention. A nanoparticle is a tiny particle with at least one dimension < 100 nm. Currently, the research on nanoparticle is a hot topic due to the extensive diversity of potential practice in electronic, optical, and biomedical fields. The nanofluid model was first established by Choi [20]. Khanafer et al. [21] were the first authors who inspected heat transfer enhancement of using nanofluids inside an enclosure with attention to solid particle dispersion. Later on, many authors investigated the influence of using nanoparticles for different fluid models. The broad range of current and future applications involving nanofluids can be found in the recent books by Das et al. [22], Shenoy et al. [23], Nield and Bejan [8], and

* Corresponding author.
E-mail addresses: mohammad.ghalambaz@tdtu.edu.vn (M. Ghalambaz), popm.ioan@yahoo.co.uk (I. Pop).

https://doi.org/10.1016/j.molliq.2019.111432
0167-7322/

Nomenclature

Latin letters

C_f	skin friction
Cp	sensible specific heat (J/kg·K)
f	similarity variable
f_1, f_2, f_3	first order ode variables, defined in Eq. (36)
g	gravitational constant (m/s^2)
h	convective heat transfer coefficient (W/m^2·K)
h_{sf}	latent heat of fusion (J/kg·K)
k	thermal conductivity coefficient (W/m K)
Nc	number of thermal conductivity
Nur	reduced Nusselt number
Nu_x	local Nusselt number
Nv	number of dynamic viscosity
Pe_x	local Peclet number
Ste	Stefan number
Ra_x	Rayleigh number
T	temperature (°C)
T_∞	external flow temperature (°C)
T_f	fusion temperature (°C)
T_{Mr}	fusion temperature range (°C)
T_w	vertical plate temperature (°C)
u	velocity component along with the plate (m/s)
U_∞	uniform external velocity (m/s)
v	velocity component perpendicular to plate (m/s)
x	the Cartesian coordinate perpendicular to the plate (m)
y	the Cartesian coordinate along with the plate (m)

Greek symbols

μ	dynamic viscosity of fluid (kg·s/m)
α	thermal diffusivity (m^2/s)
β	the coefficient of thermal-expansion (K^{-1})
γ	non-dimensional heat capacity ratio
κ	permeability of porous medium (m^2)
δ	dimensionless fusion interval
ε	porosity of the porous medium
η	non-dimensional similarity variable
θ	dimensionless temperature
θ_f	dimensionless fusion temperature
ι	the weight ratio of core to shell
λ_1, λ_2	mixing parameter
ξ	the non-dimensional specific function introduced, Eq. (23)
ρ	density (kg/m^3)
τ_w	surface shear stress (Pa)
ϕ	volume-fraction of particles
ψ	non-dimensional stream-function

Subscript

b	bulk properties of the NEPCM and host fluid
c	the capsulated PCM core
f	base fluid
m	effective of the suspension and porous matrix
p	nano-encapsulated particles (NEPCMs)
s	capsule-shell
sp	porous matrix

Superscript

$'$	differentiation respect to η

Minkowycz et al. [24] and in the review papers by Buongiorno et al. [25], Kakaç and Pramuanjaroenkij [26], Mahian et al. [27], Sheikholeslami and Ganji [28], Groşan et al. [29], Ahmadi et al. [30], Mahian et al. [31,32] and etc. There are also excellence studies in the phase change heat transfer of phase change materials [33–35] and nano-enhanced phase change materials [36,37] in enclosures.

A new type of micro/nano particles are the encapsulated phase change materials. In the encapsulation method, the core of the particles is consist of a phase change material (PCM) that is encapsulated in a shell made of polymer or in a porous matrix. The PCMs have the capability of releasing/storing a considerable amount of latent heat on phase change. Using encapsulation method has the advantage of preventing leakage of phase change materials and increasing the effective heat transfer surface.

Recently, many researchers have developed and synthesized various types of encapsulated phase change materials. For example, Wickramaratne et al. [38,39] synthesized an encapsulated chloride-based inorganic PCM for high-temperature thermal energy storage systems. They reported that the encapsulation was remained intact during 150 thermal cycles. Zhu et al. [40] successfully fabricated nano-encapsulated materials with a polymer-SiO_2 as a hybrid. Using the shell provides an enhanced leakage proof property. Zhao et al. [41] reported the fabrication of micro-encapsulated phase change materials (MEPCMs) by using titania-polyurea (TiO_2-PUA) shell.

Zhu et al. [42] fabricated nano-encapsulated phase change materials (NEPCMs) with a highly thermal conductive shell (made of Ag) and small capsule size for fast heat transfer. The core PCM was made of n-octacosane, which provides low fusion temperature. Navarrete et al. [43] utilized nano-encapsulation method for energy storage in high-temperature solar systems. Du et al. [44] encapsulated n-octadecane PCMs in a shell of PNDA-modified melamine–formaldehyde with flame retardant properties.

Regarding a suspension of NEPCM particles in a host fluid, Barlak et al. [39] synthesized a nanofluid suspension of NEPCMs in water and ethylene glycol. The nanoparticles were made of n-nonadecane as phase change material and a polymer (polyurethane) as the shell. They measured the thermal conductivity and dynamic viscosity of the suspension. The outcomes show that the presence of NEPCM particles can enhance the thermal conductivity of the water base fluid about 20% by using only 3.36% of NEPCM particles. Ghalambaz et al. [45] modeled the natural convective heat transfer of NEPCMs in a cavity with temperature difference at the side walls. The results show that the fusion temperature of the NEPCMs plays a key role in the thermal enchantment of using NEPCMs in natural convection flows. It was also found that using NEPCM particles can enhance the overall natural convection heat transfer up to 10%.

Based on the literature review, the effect of using a NEPCM suspension on the flow and heat transfer in a porous medium has not been addressed yet. The present study aims to analyze the effect of using a suspension of NEPCMs in a saturated porous medium. The case of a vertical flat plate embedded in a saturated porous medium is adapted to address the following key questions:

1- Does using NEPCMs enhance the steady convective heat transfer in a porous medium?
2- How the fusion temperature of NEPCM cores affects the heat transfer performance?
3- Does the flow regime (mixed convection) affect the NEPCMs heat transfer performance of using NEPCMs in a porous medium?

By considering the above questions, the following sections aim to model and analyze the boundary layer flow and heat transfer of NEPCMs in a porous medium.

2. Mathematical model

There is a two-dimensional steady-state and incompressible Darcy flow over a vertical flat plate. The plate is embedded in a homogeneous Darcy porous medium that is filled with a suspension of NEPCM

nanofluid. The NECPM particles are made of a core PCM and an encapsulated shell. The core of the NEPCMs undergoes phase at a fusion temperature equal to T_f. When the temperature of the fluid is higher than the fusion temperature ($T > T_f$), the core of nanoparticles will be at the liquid state. When the temperature of the liquid is lower than the fusion temperature ($T < T_f$) the core of nanoparticles will be at the solid state.

As the nanoparticles move with the fluid, they can experience cold and hot regions in the boundary layer over the plate. During the phase change, the core of NEPCMs absorbs/release a notable amount of the latent heat energy. The core of NEPCMs is commonly made of paraffin, and the shell is made of polymers. Fig. 1 depicts a schematic view of the physical model. The origin of the coordinate system is at the bottom of the plate, which x coordinate is along with the plate in the upward direction, and y coordinate is normal to the plate surface.

There is a uniform flow of NEPCM nanofluid in the porous space in an upward direction with a constant temperature of T_∞ and a constant velocity of U_∞. The plate surface is at an isothermal temperature of T_w. Considering the gravity force in the downward direction, the presence of a temperature difference between the plate surface and the uniform NEPCM nanofluid flow induces a natural convection flow. When $T_w > T_\infty$, the induced buoyancy flow is in an upward direction, which results in an assisting secondary flow. However, when $T_w < T_\infty$ the natural flow is in a downward direction, which results in an opposing flow. In the present study, it is assumed that the NEPCM nanofluid is stable and uniform. The fusion temperature of nanoparticles is higher than the plate temperature and lower than the ambient temperature ($T_w < T_f < T_\infty$), and hence, the nanoparticles will experience phase change in the boundary layer.

The porous medium matrix is treated properly, and hence, there is no sedimentation over the porous matrix. It is also assumed that the temperature difference is limited, and hence, the Oberbeck-Boussinesq approximation is valid. Considering these assumptions and applying the usual boundary layer approximations the governing equations for continuity of the NEPCM nanofluid, momentum and heat transfer are written in the porous space as [46–48]:

$$\frac{\partial u}{\partial x} + \frac{\partial v}{\partial y} = 0, \tag{1}$$

$$\frac{\mu_b}{\mu_f}\frac{\partial u}{\partial y} = \frac{g\kappa\left[\phi\rho_p\beta_p + (1-\phi)\rho_f\beta_f\right]}{\mu_f}\frac{\partial T}{\partial y} \tag{2}$$

$$(\rho c_p)_b\left(u\frac{\partial T}{\partial x} + v\frac{\partial T}{\partial y}\right) = k_{m,b}\frac{\partial^2 T}{\partial y^2} \tag{3}$$

subject to:

$$y = 0: \quad v = 0, \quad T = T_w, y\to\infty: \quad u = U_\infty, \quad T = T_\infty. \tag{4}$$

In these equations, u and v are the velocities in y and x directions, T is the fluid temperature, g is the gravity-constant in y-direction, β is the thermal expansion coefficient, ρ is the density, μ is the dynamic viscosity, c_p is the specific heat capacity, and α is the thermal diffusivity. In the above equations, the bulk suspension of NEPCM and base fluid is indicated by the subscript of b. The subscripts of f and p denote the base fluid and NEPCM particles. The subscript of m indicates the effective thermophysical properties of the NEPCM suspension and the porous matrix. Here, $k_{m,b}$ is the thermal conductivity of the NEPCM solution

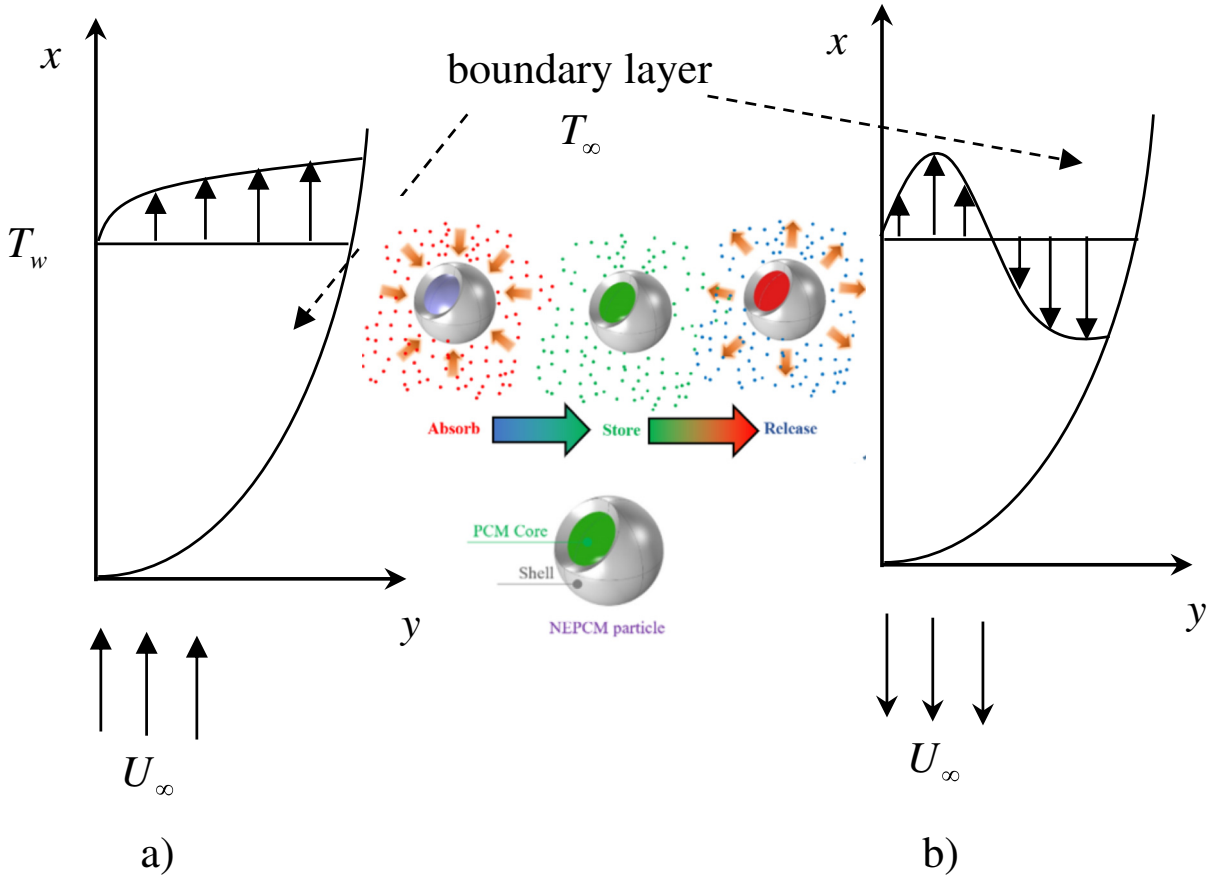

Fig. 1. Physical model and coordinate system of NEPCMs suspension over a plate embedded in a porous medium. a) Assisting flow; b) opposing flow.

and porous matrix. It is more convenient to integrate Eq. (2) along with the boundary condition of Eq. (4), which results in:

$$\frac{\mu_b}{\mu_f}u = \frac{\mu_b}{\mu_f}U_\infty + \frac{g\kappa\left[\phi\rho_p\beta_p + (1-\phi)\rho_f\beta_f\right]}{\mu_f}(T-T_\infty) \tag{5}$$

Considering the suspension of a base fluid and NEPCM nanoparticles as a nanofluid, the relations for estimation of thermophysical properties are essential. The NEPCMs is a stable solution of nanoparticles and the base fluid; hence, the density of the suspension is evaluated as Chai et al. [49]:

$$\rho_b = (1-\phi)\rho_f + \phi\rho_p \tag{6}$$

where ρ is the density and ϕ is the volume fraction of dispersed NEPCM particles. The subscripts of f and p denote the base fluid and the NEPCM nanoparticles. As mentioned, NEPCM particles are a composite of a shell and a core [44,49]. The effective density of a composite of the shell and core is calculated as [49,50]:

$$\rho_p = \frac{(1+\iota)\rho_c\rho_s}{\rho_s + \iota\rho_c} \tag{7}$$

where ι denotes the core-shell weight-ratio, and the subscript of c and s represent the core and the shell of NEPCM particles, respectively. In the cases that the experimental data are available, the density of NEPCM particles also can be measured directly, for example, by a pycnometer [39]. There can be a difference between the liquid and solid density and heat capacity of the core PCM due to the phase change; hence the average density and heat capacity of liquid and solid is adopted as the average density and heat capacity of core PCM. Based on the law of energy conservation, the specific heat capacity of a suspension of particles and a host fluid is computed by [51]:

$$Cp_b = \frac{(1-\phi)\rho_f Cp_f + \phi\rho_p Cp_p}{\rho_b} \tag{8}$$

Accordingly, in the absence of phase change, the effective specific heat-capacity of the composite NEPCM nanoparticle, which includes the core and the shell, is calculated as [50]:

$$Cp_p = \frac{(Cp_c + \iota Cp_s)\rho_c\rho_s}{(\rho_s + \iota\rho_c)\rho_p} \tag{9}$$

where the Cp_c denotes the average heat-capacity of the phase change core. It should be noted that the latent heat of the phase change is required to be considered as a part of the specific heat of the encapsulated particles.

The nanoparticles are very small in size, and hence, the phase change of nanoparticles' core in the radial direction can be neglected inside the particle. This way, a lamp model introduces the phase change of nanoparticles. The time scale of the phase change of nanoparticles is assumed much smaller than the natural convection time scale in the cavity. Thus, it is assumed that the phase change of nanoparticle occurs instantly and controlled by the temperature gradient. Accordingly, the effect of nanoparticles phase change is solely included in the effective heat capacity of the nanofluid.

In practice, pure substances undergo phase change in a fixed temperature for a fixed pressure. However, the mixtures may experience a range of temperature for phase change. Considering a fixed temperature for the phase change induces a jump in the heat equation, which will be hard to deal with regular numerical methods. Hence, following the literature studies [49,52,53], a very narrow range of phase change in adopted for the phase change of NEPCMs. Various temperature dependent profiles for describing the latent heat of phase change in the form of specific heat as a function of temperature can be assumed. The study of Alisetti and Roy [54] reveals that there is not much difference (<4%) in results by selecting different phase change profiles to describe the specific heat of phase change. Therefore, here, a sine shape profile is used due to its numerical advantages [54]:

$$Cp_c = Cp_{c,l} + \left\{\frac{\pi}{2}\cdot\left(\frac{h_{sf}}{T_{Mr}} - Cp_c\right)\cdot \sin\left(\pi\frac{T-(T_f-T_{Mr}/2)}{T_{Mr}}\right)\right\} \times \begin{cases} 0 & T<T_f-T_{Mr}/2 \\ 1 & T_f-T_{Mr}/2<T<T_f+T_{Mr}/2 \\ 0 & T>T_f+T_{Mr}/2 \end{cases} \tag{10}$$

where T_{Mr} is the fusion temperature range and T_f is the fusion temperature. If $T_{Mr} \to 0$ then $T \to T_f$ which recovers the fixed fusion temperature of phase change. The above equation shows that fusion occurs in a range of temperature, T_{Mr}. For a temperature less than $T_f - T_{Mr}/2$ and higher than $T_f + T_{Mr}/2$, the encapsulated cores are in solid and liquid phases, respectively. Now, Eq. (10) can be substituted in Eq. (9) for total specific heat capacity consisting of sensible heat and the latent heat of fusion.

The thermal volume-expansion of the suspension of a host fluid and nanoparticles (β_b) is evaluated by [51]:

$$\beta_b = (1-\phi)\beta_f + \phi\beta_p \tag{11}$$

where it is assumed that the NEPCMs are expanded the same as the regular nanoparticles.

Following studies of Buongiorno et al. [55] and Venerus et al. [56], as well as, Ghalambaz et al. [57] and Zaraki et al. [58], the volume fraction of nanoparticles changes the e dynamic viscosity/thermal conductivity linearly:

$$\frac{\mu_b}{\mu_f} = 1 + Nv\phi$$

$$\frac{k_b}{k_f} = 1 + Nc\phi \tag{12a}$$

where Nv and Nc are the number of dynamic viscosity and the number of thermal conductivity, respectively. Buongiorno et al. [55], in the form of an International Nanofluid Property Benchmark Exercise (INPBE), investigated the thermal conductivity of nanofluid samples by about 30 organizations worldwide. The measurements were performed by a variety of experimental approaches, including the optical methods, steady-state methods, and transient hot-wire method. A linear relation between the thermal conductivity and volume fraction of nanoparticles were observed. As a part of INPBE, the dynamic viscosity of some nanofluid samples were also measured [56]. Based on the outcomes, a linear relationship between dynamic viscosity and volume fraction of nanoparticles can be concluded. Therefore, in the present study linear relations of Eqs. (12a) and (12b) are adopted. Although Eqs. (12a) and (12b) are linear equations, the number of dynamic viscosity (Nv) and the number of thermal conductivity (Nc) are a function of various parameters such as the size of nanoparticles, type of nanoparticles, synthesis methods, additives, temperature and the type of the host fluid. However, for a synthesized suspension, these parameters are fixed; and hence, the value of Nc and Nv are also fixed. Barlak et al. [39] experimentally measured the thermal conductivity and dynamic viscosity of a suspension of n-nonadecane in water. By using curve fitting on experimental data of Barlak et al. [39], the number of dynamic viscosity and the number of thermal conductivity are obtained as $Nv = 12.5$ and $Nc = 23.8$. It should be noted that the introduced relations, Eqs. (12a) and (12b), are practical for a dilute suspension of nanoparticles ($\phi < 5\%$).

The effective thermal conductivity of the NEPCM suspension and porous media can be evaluated using:

$$k_{m,b} = \varepsilon k_b + (1-\varepsilon)k_{sp} \tag{13}$$

where ε is the porosity of the porous medium, and subscripts of sp is the solid matrix of the porous medium. By using Eq. (13), ratio of $k_{m,b}/k_{m,f}$ can be written as:

$$\frac{k_{m,b}}{k_{m,f}} = \frac{\varepsilon\left(k_f(1+Nc\phi)\right)+(1-\varepsilon)k_{sp}}{\varepsilon k_f+(1-\varepsilon)k_{sp}} = 1+\frac{Nc\phi}{1+\frac{(1-\varepsilon)}{\varepsilon}\left(k_{sp}/k_f\right)} \tag{14}$$

In order to reduce the governing partial differential equations of Eqs. (1), (3), (5) to a set of ordinary differential equations, the following similarity variables are introduced:

$$\psi = \alpha_{m,f}(2Pe_x)^{\frac{1}{2}} f(\eta), \qquad \theta(\eta) = (T-T_\infty)/(T_w-T_\infty), \qquad \eta = Pe_x^{\frac{1}{2}} y/\left(x\sqrt{2}\right) \tag{15}$$

where $\alpha_{m,b} = k_{m,b}/(\rho Cp)_b$ and $Pe_x = U_\infty x/\alpha_{m,f}$ is the local Peclet number for porous medium. Here, ψ is the stream function defined as $u = \partial\psi/\partial y$ and $v = -\partial\psi/\partial x$. Using the definition of ψ ensures the satisfaction of the continuity equation Eq. (1). Invoking the similarity variables, Eqs. (5) and (3) are reduced to the following set of ordinary differential equations:

$$f' = 1+\lambda_1\lambda_2\theta \tag{16}$$

$$\left(\frac{k_{m,b}}{k_{m,f}}\right)\theta'' + \frac{(\rho Cp)_p}{(\rho Cp)_f} f\theta' = 0 \tag{17}$$

subject to:

$$\begin{array}{lll} at & \eta = 0: & f(0)=0, \quad \theta(0)=1, \\ at & \eta\to\infty: & f'(\eta)\to 1, \quad \theta(\eta)\to 0. \end{array} \tag{18}$$

where

$$\lambda_1 = \frac{Ra_x}{Pe_x} = \frac{\rho_f\beta_f g\kappa(T_w-T_\infty)}{U_\infty\mu_f} \text{ and } \lambda_2 = \frac{\mu_f}{\mu_b}\left((1-\phi)+\phi\frac{(\rho\beta)_s}{(\rho\beta)_f}\right) \tag{19}$$

where $Ra_x = \rho_f g\beta_f\kappa(T-T_\infty)x/\mu_f\alpha_{m,f}$ is the local Darcy-Rayleigh number. In Eq. (19), λ_2 denotes the effect of the presence of NEPCM nanoparticles on the buoyancy force. Now, combining Eqs. (16) and (17) along with their boundary conditions, Eq. (18), results in:

$$\left(\frac{k_{m,b}}{k_{m,f}}\right)f''' + \frac{(\rho Cp)_p}{(\rho Cp)_f} f f'' = 0 \tag{20}$$

$$f(0)=0,\ f'(0)=1+\lambda_1\lambda_2, \text{ and } f'(\infty)=1 \tag{21}$$

Now, by introducing the following non-dimensional parameters:

$$\theta_f = \frac{T_f-T_c}{T_w-T_c}, \quad \delta = \frac{T_{Mr}}{T_w-T_c} \tag{22}$$

Eq. (10) can be written in a non-dimensional form as:

$$\xi = \frac{\pi}{2}\sin\left(\frac{\pi}{\delta}\left(\theta-\theta_f+\frac{\delta}{2}\right)\right) \times \begin{cases} 0 & \theta<\theta_f-\frac{\delta}{2} \\ 1 & \theta_f-\frac{\delta}{2}<\theta<\theta_f+\frac{\delta}{2} \\ 0 & \end{cases} \tag{23}$$

and accordingly using Eqs. (8)–(10), the term $(\rho c_p)_b/(\rho c_p)_f$ is obtained as:

$$\frac{(\rho Cp)_b}{(\rho Cp)_f} = (1-\phi)+\phi\frac{(Cp_c+\iota Cp_s)\rho_c\rho_s}{Cp_f(\rho_s+\iota\rho_c)\rho_f} + \phi\frac{(T_w-T_C)}{T_{Mr}}\left\{\frac{\pi\rho_c\rho_s}{2Cp_f(\rho_s+\iota\rho_c)\rho_f}\left(\frac{h_{sf}-Cp_cT_{Mr}}{(T_w-T_\infty)}\right)\right\}\xi \tag{24}$$

In the above equation, the term $[(\rho_c\rho_s)(h_{sf}-Cp_cT_{Mr})]/[(T_w-T_\infty)(Cp_f(\rho_s+\iota\rho_c)\rho_f)]$ includes both of the sensible heat and the latent heat terms. As mentioned, T_{Mr} represents the phase-change temperature-interval, which is a narrow interval. Besides, Cp_c, which is the sensible heat, is much smaller than the latent heat, h_{fs}. Therefore, the combination of $Cp_c \times T_{Mr}$ is a negligible term compared to h_{sf}. By neglecting this term, the Stefan number is defined as regular as:

$$Ste = \frac{(\rho Cp)_f(T_w-T_\infty)(\rho_s+\iota\rho_c)}{(h_{sf}\rho_c\rho_s)} \tag{25}$$

Consequently, the term $(\rho c_p)_b/(\rho c_p)_f$ is re-written in the non-dimensional as:

$$\frac{(\rho Cp)_b}{(\rho Cp)_f} = (1-\phi)+\phi\gamma+\frac{\phi}{\delta Ste}\xi \tag{26}$$

where γ is the heat capacity ratio defined as:

$$\gamma = \frac{(Cp_c+\iota Cp_s)\rho_c\rho_s}{(\rho Cp)_f(\rho_s+\iota\rho_c)} \tag{27}$$

Substituting the ratio terms of $(\rho c_p)_b/(\rho c_p)_f$ and $k_{m,b}/k_{m,f}$ from Eqs. (14) and (26) in Eq. (20) results in:

$$\left(1+\frac{Nc\phi}{1+\frac{(1-\varepsilon)}{\varepsilon}\left(k_{sp}/k_f\right)}\right)f''' + \left((1-\phi)+\phi\gamma+\frac{\phi}{\delta Ste}\xi\right)f f'' = 0 \tag{28}$$

Invoking Eqs. (12b) and (19), the boundary conditions Eq. (21) is re-written as:

$$f(0)=0, \qquad f'(0) = 1+\lambda_1\frac{1-\phi+\phi\left((\rho\beta)_p/(\rho\beta)_f\right)}{1+Nv\phi} \quad \text{and } f'(\eta)\to 1 \quad as \quad \eta\to\infty \tag{29}$$

where λ_1 is the constant mixed convection parameter.

The parameter of interest is the surface heat transfer. At the wall surface, the heat conduction $(-k_{m,b}\times\partial T/\partial y)$ is equal to the convective heat transfer, i.e. $h(T_w-T_\infty)$, due to energy balance where h is the coefficient of convective heat transfer at the plate surface. Thus, employing the similarity variables of Eq. (15), the local Nusselt number ($Nu_x = h\,x/k_{m,f}$) and reduced Nusselt number (Nur) are obtained as:

$$Nur = \sqrt{2}\lambda_1 Nu_x Pe_x^{-\frac{1}{2}} = -\frac{k_{m,b}}{\lambda_2 k_{m,f}} f''(0) \tag{30}$$

where using Eqs. (12a) and (12b) it can be rewritten as:

$$Nur = -\left(1+\frac{Nc\phi}{1+\frac{(1-\varepsilon)}{\varepsilon}\left(k_{sp}/k_f\right)}\right)\left(\frac{1-\phi+\phi\frac{(\rho\beta)_p}{(\rho\beta)_f}}{1+Nv\phi}\right)^{-1} f''(0) \tag{31}$$

where Nur denotes the reduced Nusselt number at the plate surface. It is worth noticing that the temperature gradient at the wall surface $\theta'(0)$ is

related to the stream function variable of f as

$$\theta'(0) = \lambda_1^{-1}\lambda_2^{-1} f''(0) \tag{32}$$

Skin friction coefficient, C_f, is introduced as

$$C_f = \frac{\tau_w}{\rho_f U_\infty^2} \tag{33}$$

where $\tau\tau_w$ is the skin friction or shear stress along with the plate, that is given by

$$\tau_w = \mu_b \left(\frac{\partial u}{\partial y}\right)_{y=0} \tag{34}$$

Using Eq. (33) and similarity variables, the skin fraction can be written as:

$$\frac{1}{\sqrt{2}}C_f = \frac{\mu_b}{\mu_f} f''(0) = (1 + Nv\phi) f''(0) \tag{35}$$

3. Numerical method and code validation

The third order non-linear boundary value ordinary differential equation, Eq. (28), along with the set of boundary conditions of Eq. (29) is solved by a finite-difference solver bvp4c code. Following bvp4c code, Eqs. (28) and (29) are written as the following set of first-order non-linear equations:

$$\begin{aligned} df_1 &= f_2 \\ df_2 &= f_3 \\ df_3 &= \frac{-\left((1-\phi) + \phi\gamma + \frac{\phi}{\delta Ste}\xi\right) f_1 f_3}{1 + \frac{Nc\phi}{1 + \frac{(1-\varepsilon)}{\varepsilon}(k_s/k_f)}} \end{aligned} \tag{36}$$

subject to:

$$f_1(0) = 0, \qquad f_2(0) = 1 + \lambda_1 \frac{1 - \phi + \phi\left((\rho\beta)_p/(\rho\beta)_f\right)}{1 + Nv\phi} \quad \text{and} \quad f_1(\eta) \to 1 \quad as \quad \eta \to \infty \tag{37}$$

A collocation method with automatic grid adaptation is utilized to control the error and convergence of the solution in the finite difference method. The Newton method as an iterative method is utilized to solve the algebraic residual equations. The calculations are continued until a relative error $< 10^{-9}$ is reached. The appropriate selection of the asymptotic value of the boundary condition is very important for numerical calculations. The asymptotic value of $\eta_\infty = 12$ is adopted for calculations to ensure that the results are independent of the asymptotic value of the boundary conditions at the edge of the boundary layer. It is also found that the present study has a dual solution. To capture both solutions, a continuation approach is employed by using suitable initial guesses.

To ensure the performance of the developed code, the study of Merkin [14] is selected as a benchmark study. The results of the present study are compared outcomes of Merkin [14] when $\phi = 0$, and the results are summarized in Table 1.

Table 1
Validation against Merkin [14] when $\phi = 0$.

λ_1	Merkin [14]	Present	Merkin [14]	Present
	$f_{upper}''(0)$	$f_{upper}''(0)$	$f_{lower}''(0)$	$f_{lower}''(0)$
−1.000	0.46960	0.469600		
−1.100	0.46105	0.461049	0.00194	0.001936
−1.200	0.43015	0.430151	0.02219	0.022188
−1.300	0.35664	0.356638	0.08497	0.084889
−1.350	0.25758	0.257581	0.17856	0.178597
−1.354	0.22428	0.224296		

4. Results and discussion

As a case study, the suspension of polyurethane (PU) and nonadecane as encapsulated nanoparticles, and water as the host fluid are adopted. The NEPCM particles are made of nonadecane as phase change core and polyurethane as shell [39].

The volume fraction of NEPCM particles is in the range of $0 < \phi < 0.05$, which corresponds to a dilute suspension NEPCMs in water. Following Barlak et al. [39], N-nonadecane is adopted as the PCM core, polyurethane is selected as the shell material for the encapsulated particles, and the host fluid is water. As Barlak et al. [39] reported, the fusion temperature of NEPCM particles was about 32 °C, and the average latent heat of nonadecane fusion was about 211 kJ/kg. The core-shell weight ratio was estimated as $\iota \sim 0.447$. The densities of polyurethane, n-nonadecane, and PU-nonadecane NEPCM particles are adopted as 721 (kg/m^3) and 786 (kg/m^3), and 1190 (kg/m^3), respectively. The specified heat capacities of polyurethane (PU) are adopted as 1317 (J/kg K). The specific heat of n-nonadecane [59] is 2037 (J/kg K). Assuming $T_w - T_\infty$ as 10 K, the heat capacity ratio (γ) and Stephan number (*Ste*) are evaluated as $\gamma = 0.333$ and $Ste = 0.3355$. The dimensionless fusion-temperature is selected in the interval of $0 < \theta_f < 1$.

Following the experimental study of Barlak et al. [39], the number of dynamic viscosity and the number of thermal conductivity are approximated as $Nv \sim 12.5$ and $Nc \sim 23.8$ for the suspension of PU-nonadecane in water. The volume thermal expansion coefficient for polyurethane is $3 \times 57.6 \times 10^{-6}$ (1/K) and for water is 210 (1/K) $\times 10^{-6}$; thus, the term $(\rho\beta)_p/(\rho\beta)_f$ is calculated as 1.018. Assuming the permeability of porous space as 10^{-6} (m^2) and uniform flow velocity of $U_\infty = 0.01$ m/s, λ_1 is a small value in the order of 0.01. The thermal conductivity ratio of k_s/k_f can be varied in the range of 0.1 to 100 depending on the thermal conductivity of the porous medium. The porosity can be varied in the range of 0 to 1, which zero indicates no void space and 1 is the clear flow with no porous matrix. δ is the melting interval range and should be selected as a small value. Here, δ is adopted as $\delta = 0.05$.

As a summary, the non-dimensional parameters for the suspension of PU-nonadecane in water are fixed as $\iota \sim 0.447$, $Ste = 0.3355$, $\gamma = 0.333$, $Nc \sim 23.8$, $Nv \sim 12.5$ and $(\rho\beta_p)/(\rho\beta_f) = 1.018$. The default values of other parameters are adopted as $\lambda_1 = 0.01$, $k_s/k_f = 0.1$, $\varepsilon = 0.3$, $\theta_f = 0.3$ and $\phi = 2\%$. The results will be obtained from the default set of non-dimensional parameters; otherwise, it will be stated. The prefix of "non-dimensional" can be skipped as all of the equations and results will be reported in the non-dimensional form.

Fig. 2 shows the dual solution boundary layer profiles for NEPCM nanofluid when $\lambda_1 = -1.4$. Continues lines depict the stable solution while dash-lines denotes the unstable solution. The boundary layer thickness of the stable solution is lower than that of an unstable solution. In an unstable boundary layer, the environmental noises can easily distribute in the fluid and change the boundary layer to a stable boundary layer. Hence, the unstable boundary layer cannot be existing in regular domains with usual physical noises. In contrast, the noises will be damped in a stable boundary layer.

Figs. 3 and 4 show the boundary layer velocity and temperature profiles for various volume fractions of NEPCM particles. As seen, the variation of volume fraction of NEPCM particles would significantly affect the velocity and temperature boundary layer profiles. When η is about unity, all of the velocity profiles reach a focal point. Attention to Fig. 4 reveals that $\eta = 1$ corresponds to a non-dimensional temperature about $\theta = 0.3$, which is the fusion temperature of $\theta_f = 0.3$. Hence, it can be

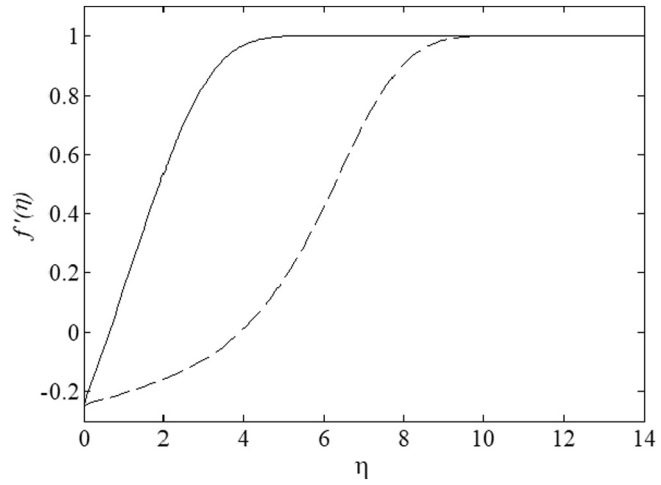

Fig. 2. Stable (full line) and unstable (broken line) velocity profiles for $\lambda_1 = -1.4$ and $\phi = 0.01$.

concluded that the behavior of the velocity profiles is dictated by the thermal boundary layer and phase change behavior of NEPCM nanoparticles. The increase of volume fraction of NEPCM particles reduces the surface velocity at the wall. It should be noted that in the Darcy flow, the wall slip velocity at the surface is possible. The reduction of the velocities at the wall is mainly due to the increase of dynamic viscosity of nanofluid by the increase of the volume fractions of nanoparticles.

Fig. 4 shows that the increase of the volume fraction of NEPCM particles increases the boundary layer thickens. This is due to the enhancement of the thermal conductivity of the solution. Moreover, in the case of $\eta = 1$, which is about the fusion temperature, a slight change in the temperature profile of $\phi = 0.05$ can be seen. In this case, the temperature profile shows that the phase change of NECPM cores tends to increase the temperature gradient at the surface.

Fig. 5 illustrates the influence of the fusion temperature on the boundary layer velocity profiles when $\lambda_1 = 1$ and $\phi = 0.05$. As seen, there is an obvious change in the velocity profiles about $\eta = 1$ to $\eta = 2$ by the change of θ_f. Tracking the changes in the velocity profiles shows that the origin of the changes shifts to lower the value of η by the increase of θ_f. This is in agreement with the results of Figs. 4 and 5 since the behavior of the hydrodynamic boundary layer is under the

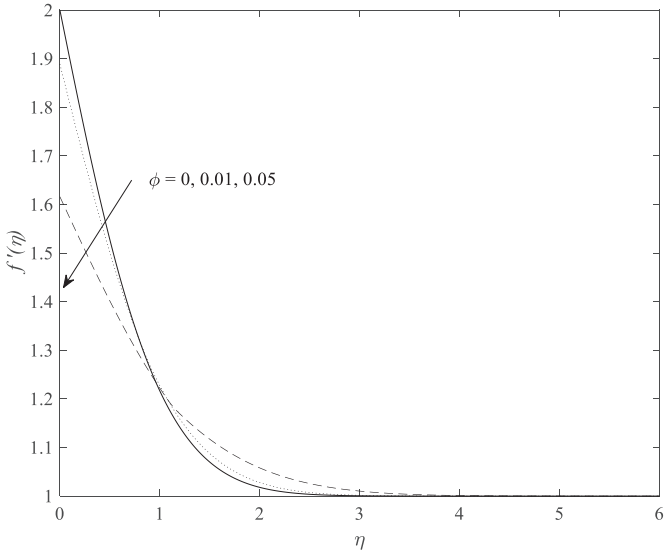

Fig. 3. Dimensionless velocity profiles for $\lambda_1 = 1$ and different values of nanoparticles concentration parameter ϕ.

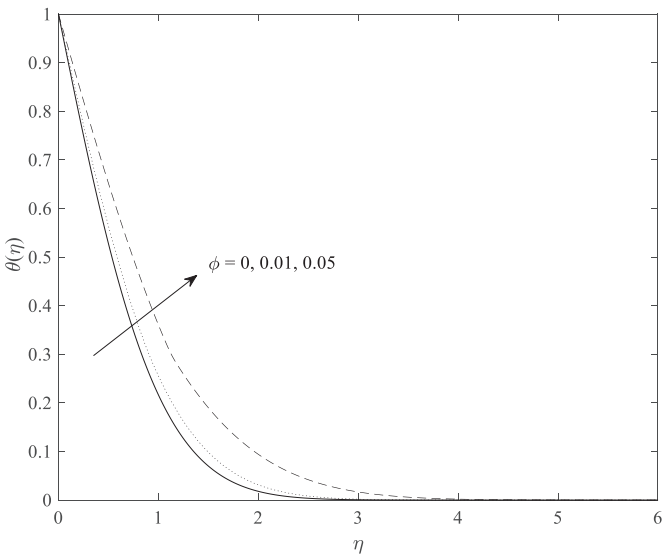

Fig. 4. Dimensionless temperature profiles for $\lambda_1 = 1$ and different values of nanoparticles concentration parameter ϕ.

significant influence of the thermal boundary layer. The phase change of NEPCM particles occurs about $\eta = 1$ to $\eta = 2$ and shifts toward the hot plate by the increase of the fusion temperature. Interestingly, the variation of the fusion temperature does not show a notable effect on the thickness of the boundary layer; however, it changes the slope of the temperature profiles at the wall by making a notable change in the asymptotic behavior of temperature profiles due to the latent heat of fusion.

The values of $f''(0)$ as a function of λ_1 are plotted in Fig. 6 for various values of volume fraction of NEPCM particles. As seen, there are two solutions for some negative values of λ_1. The critical values of λ_1 are summarized and reported in Table 2. Figs. 7 and 8 depict the non-dimensional temperature gradient $(\theta'(0))$ and Nusselt number at the wall surface for various values of λ_1. Fig. 7 illustrates the effect of volume fraction of NEPCM particles while Fig. 8 depicts the effect of fusion temperature. Fig. 7 shows that the increase of λ_1 reduces the temperature gradient at the surface. The increase of λ_1 can be considered as weakening of the forced convection power. Hence, it can be expected that the temperature gradient grows. Fig. 7 interestingly shows that the temperature gradient depends on the λ1 and the volume fractions of nanoparticles. For instance, when $\lambda_1 = -1.5$, the magnitude of temperature

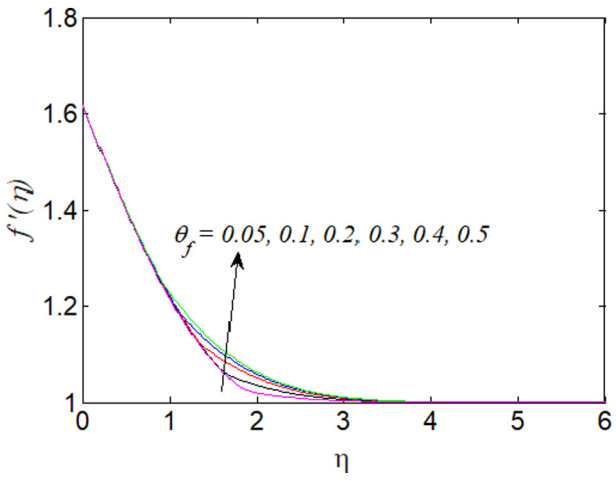

Fig. 5. Dimensionless velocity profiles for $\lambda_1 = 1$, $\phi = 0.05$ and different values of the parameter θ_f.

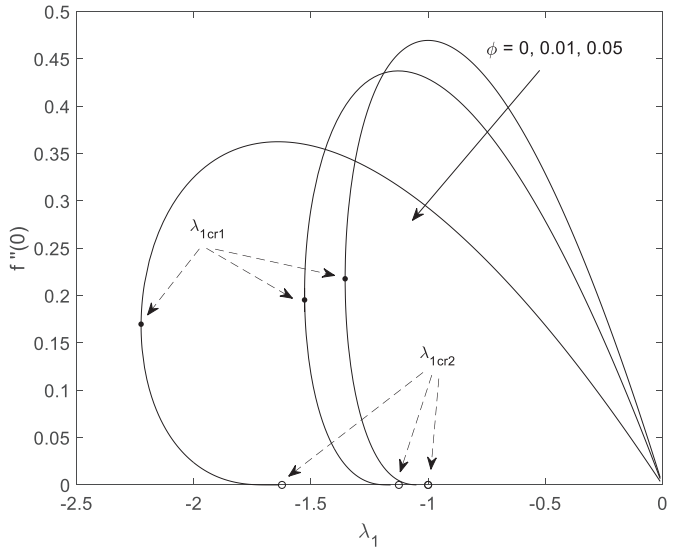

Fig. 6. Dual solution existence domain for different values of nanoparticles concentration parameter ϕ.

Table 2
The critical values of the parameter λ_1.

ϕ	λ_1	
	Critical 1	Critical 2
0	−1.3541	−1.0000
0.01	−1.5272	−1.1248
0.05	−2.2247	−1.6235

gradient in the case of zero volume fraction of nanoparticles is higher than that of $\phi = 0.05$. In contrast, when $\lambda_1 = +1$, the magnitude of temperature gradient in the case of zero volume fraction of MEPCM particles is much lower than the case of $\phi = 0.05$.

Fig. 7 shows that the increase of the volume fraction of NEPCM particles increases the temperature gradient at the wall surface for $\lambda_1 > \lambda_{1cr2}$, while the value of the Nusselt number increases for all values of λ_1. It is worth mentioning that for $\lambda_1 < \lambda_{1cr2}$ the external flow and the flow due to the buoyancy are opposite (i.e., the temperature of the wall is lower than the ambient temperature) and in this case, the magnitude of $\theta'(0)$ increases with the increase of ϕ. The decrease of the magnitude of $\theta'(0)$ by the increase of ϕ for the cases with high values of λ_1 is because the presence of nanoparticles increases the thermal conductivity of the base fluid. Hence, in a fluid with higher thermal conductivity, the temperature gradient drops. Fig. 7 also shows that the increase of the volume fraction of nanoparticles increases the Nusselt number. Although it was observed that the behavior of the temperature gradient at the wall surface depends on the value of λ_1, the behavior of the Nusselt number is monotonic with the variation of λ_1. The reason is due to the notable improvement of thermal conductivity of the NEPCM in the presence of nanoparticles. In agreement with the behavior of $\theta'(0)$, the enhancement of using nanoparticles in the low values of λ_1 is notable.

Fig. 8 shows that the increase of the fusion temperature decreases the magnitude of temperature gradient and Nusselt number in the boundary layer. The reason is the fact that by the increase of the fusion temperature, the occurrence of the phase change shifts toward the wall surface. During the phase change of MEPCM particles, the temperature would be fixed about the fusion temperature, and hence, the temperature gradient at the wall reduces. Hence, it should be noted that the presence of NEPCM particles enhances the total heat transfer in the boundary layer due to the enhancement of the thermal conductivity of the liquid. However, when the fusion temperature is high, the phase change of the nanoparticle cores deteriorates the temperature gradient and the Nusselt number.

5. Conclusion

The phase change heat transfer of NEPCMs in a porous medium is studied over a flat plate with aiding or opposing uniform external flow. The phase change of nanoparticles is modeled using a sine profile over a limited temperature range. Therefore, the heat capacity of nanoparticles is a function of temperature in the phase change range. A similarity transformation approach is successfully utilized to transform the governing equations into a non-linear differential equation. The finite difference method is utilized to solve the governing equations. The outcomes can be summarized as follows:

1- There are two solution branches in the case of strong opposing fluid. The existence of the solution branches depends on a mixing parameter λ_1. The critical value of the mixing parameter, λ_1, are derived and reported. The increase of the volume fraction of NEPCM particles increases the magnitude of the mixing parameter.
2- Based on the obtained results, the presence of NEPCM particles always enhances the heat transfer over the plate. However, the behavior of the temperature gradient as a function of the volume fraction of nanoparticles depends on the value of the mixing parameter. Hence, the mixing parameter is a key parameter on the heat transfer enhancement of using NEPCMs.
3- The decrease of the fusion-temperature of the NEPCMs, θ_f, increases the surface temperature gradient and the overall heat transfer (Nusselt number) over the plate. Hence, NEPCMs with lower fusion temperature are more of interest for heat-transfer enhancement.

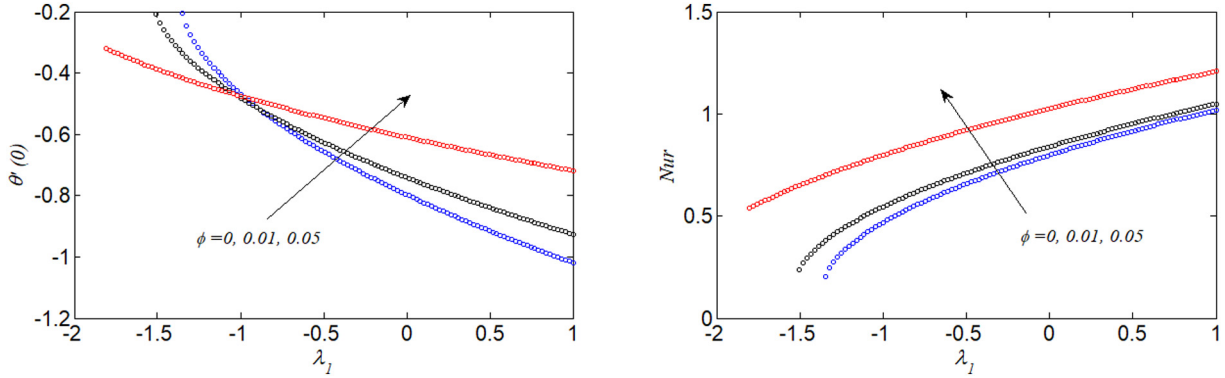

Fig. 7. Variation of $\theta'(0)$ (left) and *Nur* (right) for λ_1 when $\theta_f = 0.8$.

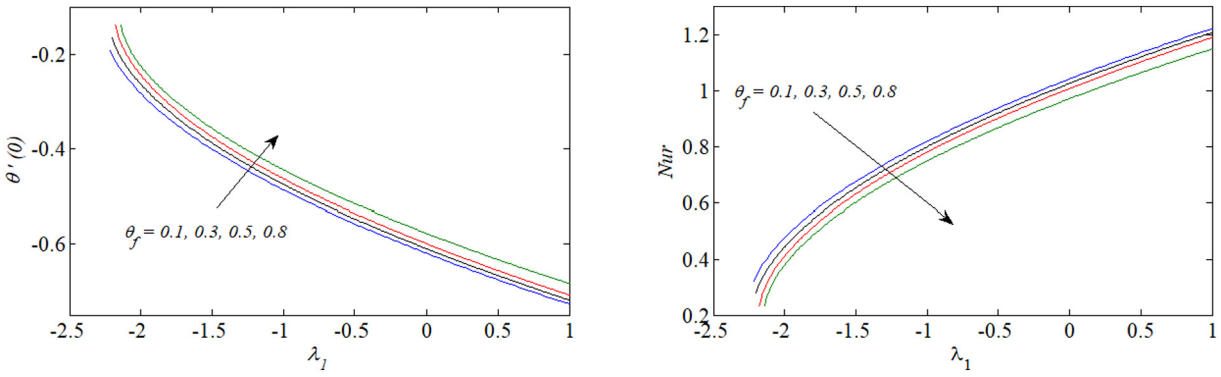

Fig. 8. Variation of $\theta'(0)$ (left) and *Nur* (right) for λ_1 when $\phi = 0.05$.

In the present work, the temperature of the hot plate was considered to be constant, and the effect of using NEPCM particles on the heat transfer was studied. In much practical application, including the cooling of electronic components or solar applications, the plate can be exposed to a constant heat flux. In this case, the uniformity of the temperature at the surface or surface temperature is of interest. Hence, the study of the boundary layer behavior of NEPCMs over a flat plate with a constant heat flux can be subject of future studies.

Acknowledgments

This work of M. Ghalambaz was supported by the STAR Institute - UBB, Cluj-Napoca, Romania, External Fellowship program, and the work by T. Groşan and I. Pop has been supported from the Grant PN-III-P4-IDPCE-2016-0036, UEFISCDI, Romanian Ministry of Sciences.

References

[1] P, Cheng, Elsevier, Advances in Heat Transfer, 1979 1–105.
[2] P. Cheng, Natural Convection: Fundamentals and Applications, 1985.
[3] Sadık Kakaç, Ramesh K. Shah, Win Aung, Handbook of single-phase convective heat transfer, Wiley-Interscience, 1987.
[4] I. Pop, D.B. Ingham, Convective Heat Transfer: Mathematical and Computational Modelling of Viscous Fluids and Porous Media, Elsevier, 2001.
[5] D.B. Ingham, I. Pop, Transport Phenomena in Porous Media III, Elsevier, 2005.
[6] D.B. Ingham, I. Pop, Transport Phenomena in Porous Media III, Elsevier, 2002.
[7] D.B. Ingham, I. Pop, Transport Phenomena in Porous Media III, Elsevier, 1998.
[8] D.A. Nield, A. Bejan, Convection in Porous Media. 4 edn, Springer, 2013.
[9] A. Bejan, I. Dincer, S. Lorente, A. Miguel, H. Reis, Porous and Complex Flow Structures in Modern Technologies, Springer Science & Business Media, 2013.
[10] K. Vafai, Handbook of Porous Media, Crc Press, 2015.
[11] K. Vafai, Porous Media: Applications in Biological Systems and Biotechnology, CRC Press, 2010.
[12] P. Vadász, Emerging Topics in Heat and Mass Transfer in Porous Media: From Bioengineering and Microelectronics to Nanotechnology, Springer Science & Business Media, 2008.
[13] J. Bear, Modeling Phenomena of Flow and Transport in Porous Media, Springer, 2018.
[14] J. Merkin, J. Eng. Math. 14 (1980) 301.
[15] J. Merkin, J. Eng. Math. 20 (1986) 171.
[16] D. Cimpean, J. Merkin, I. Pop, D. Ingham, Transp. Porous Media 64 (2006) 393.
[17] J. Merkin, I. Pop, Transp. Porous Media 85 (2010) 397.
[18] J.H. Merkin, A.M. Rohni, S. Ahmad, I. Pop, Transp. Porous Media 94 (2012) 133.
[19] Y. Lok, J. Merkin, I. Pop, Transp. Porous Media 98 (2013) 451.
[20] S.U. Choi, J.A. Eastman, Argonne National Lab, IL (United States), 1995.
[21] K. Khanafer, K. Vafai, M. Lightstone, Int. J. Heat Mass Transf. 46 (2003) 3639.
[22] S.K. Das, S.U. Choi, W. Yu, T. Pradeep, Nanofluids: Science and Technology, John Wiley & Sons, 2007.
[23] A. Shenoy, M. Sheremet, I. Pop, Convective Flow and Heat Transfer From Wavy Surfaces: Viscous Fluids, Porous Media, and Nanofluids, CRC Press, 2016.
[24] W. Minkowycz, E. Sparrow, J.P. Abraham, Nanoparticle Heat Transfer and Fluid Flow. CRC Press, 2013.
[25] J. Buongiorno, J. Heat Transf. 128 (2006) 240.
[26] S. Kakaç, A. Pramuanjaroenkij, Int. J. Heat Mass Transf. 52 (2009) 3187.
[27] O. Mahian, A. Kianifar, S.A. Kalogirou, I. Pop, S. Wongwises, Int. J. Heat Mass Transf. 57 (2013) 582.
[28] M. Sheikholeslami, D. Ganji, J. Taiwan Inst. Chem. Eng. 65 (2016) 43.
[29] T. Groşan, A.M. Sheremet, I. Pop, Advances in New Heat Transfer Fluids, CRC Press, 2017 267–286.
[30] M.H. Ahmadi, A. Mirlohi, M.A. Nazari, R. Ghasempour, J. Mol. Liq. 265 (2018) 181.
[31] O. Mahian, L. Kolsi, M. Amani, P. Estellé, G. Ahmadi, C. Kleinstreuer, J.S. Marshall, M. Siavashi, R.A. Taylor, H. Niazmand, Phys. Rep. 790 (2019) 1.
[32] O. Mahian, L. Kolsi, M. Amani, P. Estellé, G. Ahmadi, C. Kleinstreuer, J.S. Marshall, R.A. Taylor, E. Abu-Nada, S. Rashidi, Phys. Rep. 791 (2019) 1.
[33] N.S. Bondareva, M.A. Sheremet, Int. J. Heat Mass Transf. 124 (2018) 1275.
[34] N.S. Bondareva, M.A. Sheremet, International Heat Transfer Conference Digital Library, Begel House Inc., 2018
[35] N. Bondareva, N. Gibanov, M. Sheremet, Journal of Physics: Conference Series, IOP Publishing, 2018 012023.
[36] N.S. Bondareva, B. Buonomo, O. Manca, M.A. Sheremet, Int. J. Heat Mass Transf. 135 (2019) 1063.
[37] N.S. Bondareva, B. Buonomo, O. Manca, M.A. Sheremet, Appl. Therm. Eng. 144 (2018) 972.
[38] C. Wickramaratne, J.S. Dhau, R. Kamal, P. Myers, D. Goswami, E. Stefanakos, Appl. Energy 221 (2018) 587.
[39] S. Barlak, O.N. Sara, A. Karaipekli, S. Yapıcı, Nanoscale Microscale Thermophys. Eng. 20 (2016) 85.
[40] Y. Zhu, Y. Qin, C. Wei, S. Liang, X. Luo, J. Wang, L. Zhang, Energy Convers. Manag. 164 (2018) 83.
[41] A. Zhao, J. An, J. Yang, E.-H. Yang, Appl. Energy 215 (2018) 468.
[42] Y. Zhu, Y. Chi, S. Liang, X. Luo, K. Chen, C. Tian, J. Wang, L. Zhang, Sol. Energy Mater. Sol. Cells 176 (2018) 212.
[43] N. Navarrete, R. Mondragón, D. Wen, M.E. Navarro, Y. Ding, J.E. Juliá, Energy 167 (2019) 912.
[44] X. Du, Y. Fang, X. Cheng, Z. Du, M. Zhou, H. Wang, ACS Sustain. Chem. Eng. 6 (2018) 15541.
[45] M. Ghalambaz, A.J. Chamkha, D. Wen, Int. J. Heat Mass Transf. 138 (2019) 738.
[46] S. Ahmad, I. Pop, Int. Commun. Heat Mass Transfer 37 (2010) 987.
[47] S. Kuravi, K.M. Kota, J. Du, L.C. Chow, Journal of Heat Transfer 131 (2009) 062901.
[48] M.M.U. Rehman, Z.G. Qu, R.P. Fu, J. Therm. Sci. 25 (2016) 431.
[49] L. Chai, R. Shaukat, L. Wang, H.S. Wang, Appl. Therm. Eng. 135 (2018) 334.
[50] B. Chen, X. Wang, R. Zeng, Y. Zhang, X. Wang, J. Niu, Y. Li, H. Di, Exp. Thermal Fluid Sci. 32 (2008) 1638.
[51] K. Khanafer, K. Vafai, Int. J. Heat Mass Transf. 54 (2011) 4410.
[52] H.R. Seyf, Z. Zhou, H. Ma, Y. Zhang, Int. J. Heat Mass Transf. 56 (2013) 561.
[53] B. Rajabifar, Int. J. Heat Mass Transf. 88 (2015) 627.
[54] E.L. Alisetti, S.K. Roy, J. Thermophys. Heat Transf. 14 (2000) 115.
[55] J. Buongiorno, D.C. Venerus, N. Prabhat, T. McKrell, J. Townsend, R. Christianson, Y.V. Tolmachev, P. Keblinski, L.W. Hu, J.L. Alvarado, I.C. Bang, J. Appl. Phys. 106 (2009) 094312.
[56] D. Venerus, J. Buongiorno, R. Christianson, J. Townsend, I.C. Bang, G. Chen, S.J. Chung, M. Chyu, H. Chen, Y. Ding, Applied Rheology, Journal 20 (4) (2010) 44582, https://doi.org/10.3933/ApplRheol-20-44582.
[57] M. Ghalambaz, A. Doostani, E. Izadpanahi, A.J. Chamkha, J. Taiwan Inst. Chem. Eng. 72 (2017) 104.
[58] A. Zaraki, M. Ghalambaz, A.J. Chamkha, M. Ghalambaz, D. De Rossi, Adv. Powder Technol. 26 (2015) 935.
[59] Y. Rao, F. Dammel, P. Stephan, G. Lin, Heat Mass Transf. 44 (2007) 175.